SF2A 2022
J. Richard, A. Siebert, E. Lagadec, N. Lagarde, O. Venot, J. Malzac, J.-B. Marquette, M. N'Diaye, D. Briot (eds)

REVISITING DISK DEMOGRAPHICS IN THE EMERGING PARADIGM OF MHD DISK WINDS

B. Tabone[1], G. P. Rosotti[2], G. Lodato[2], P. J. Armitage[3] and A. J. Cridland[4]

Abstract. The secular evolution of planet-forming disks is regulated by the extraction of angular momentum and mass-loss processes. Recently, there has been a growing recognition that magnetic outflows launched from disks (aka "MHD disk-winds") could control the extraction of angular momentum. In this contribution, we present our recent work aiming at building simple but physically motivated disk evolution models in the MHD wind-driven scenario. This model is then used to build synthetic disk populations and compare the predictions to the recent surveys of the nearby star-forming regions. We show that MHD wind-driven accretion can explain both the main features of disk dispersal (time scale and rapidity), and the correlation between accretion rates and disk masses as unveiled in the Lupus star-forming region.

Keywords: accretion disks - MHD disk winds - protoplanetary disks - submillimetre: planetary systems

1 Introduction

The final architecture of planetary systems depends on the secular evolution of disks in which they form (Morbidelli & Raymond 2016). Over the past decades, two essential features of disk evolution have been identified: first, disks as identified from their infrared excess accrete gas, implying a transport of angular momentum, and secondly, disks are dispersed after a typical time of 2-3 Myr. These two features have long been attributed to two distinct processes: the radial transport of angular momentum by MRI turbulence, and the effect of hydrodynamical photoevaporative winds. However, there has been a growing recognition that in large regions, disks are weakly turbulent (Lesur et al. 2022). As an alternative, numerical simulations and observations have shown that magnetic outflows launched from disks (aka "MHD disk-winds") could control the extraction of angular momentum (e.g., Béthune et al. 2017). If so, planet formation would be profoundly impacted as wind-driven accretion can enhance the growth rate of planetary cores, affect the migration pattern of forming planets, and control disk dispersal.

However, the presence of MHD disk-winds remains an open question. Now, near-complete surveys of multiple star-forming regions with ALMA and VLT provide us with an unprecedented statistical sample of stellar masses, mass accretion rates, and disk (dust) masses that can be used to test disk evolution models (Manara et al. 2022). These data have almost exclusively been analysed in the framework of viscous disks including the effect of photoevaporation (e.g., Lodato et al. 2017; Sellek et al. 2020). In this contribution, we present our recent work that reconsiders disk demographics in the framework of MHD wind-driven accretion. To do so, we expand the paradigmatic viscous model of Shakura & Sunyaev (1973) to wind-driven accretion and find analytical solutions that are a generalization of the Lynden-Bell & Pringle (1974) solutions (Tabone et al. 2022a). We then adopt a disk population synthesis approach to compare the prediction of the model to the disk surveys, in particular that of Lupus (Tabone et al. 2022b). We finally discuss the new avenues to better understand the secular evolution of disks, and make the link between the diversity of exoplanets and their formation.

[1] Université Paris-Saclay, CNRS, Institut d'Astrophysique Spatiale, 91405 Orsay, France
[2] Dipartimento di Fisica, Università degli Studi di Milano, Via Celoria 16, Milano, Italy
[3] Department of Physics and Astronomy, Stony Brook University, Stony Brook, NY 11794, USA; Center for Computational Astrophysics, Flatiron Institute, New York, NY 10010, USA
[4] Max-Planck-Institut für Extraterrestrishe Physik, Gießenbachstrasse 1, 85748, Garching, Germany

2 Disk evolution model

2.1 Master equations

Our disk population model is based on a new disk evolution model presented in Tabone et al. (2022a). In short, we assume a geometrically thin disk in Keplerian rotation. The evolution of the surface density can then be written as

$$\frac{\partial \Sigma}{\partial t} = \frac{2}{r}\frac{\partial}{\partial r}\left\{\frac{1}{r\Omega}\frac{\partial}{\partial r}\left(r^2\int_{-H_W}^{+H_W} T_{r\phi}dz\right)\right\} + \frac{2}{r}\frac{\partial}{\partial r}\left\{\frac{r|T_{z\phi}|_{-H_W}^{+H_W}}{\Omega}\right\} - \dot{\Sigma}_W, \tag{2.1}$$

where $T_{r\phi} \equiv < \rho v_r \delta v_\phi - B_r B_\phi/4\pi >$ is the time-averaged radial stress tensor describing the radial transport of angular momentum, $T_{z\phi} \equiv < \rho v_z \delta v_\phi - B_z B_\phi/4\pi >$ is the time-averaged vertical stress tensor describing the extraction of angular momentum by the MHD disk wind, and $\dot{\Sigma}_W$ is the mass-loss rate per unit surface induced by the wind. Here, we adopt conventional notations for a cylindrical coordinate system with $\Omega = \sqrt{GM_*/r^3}$ the Keplerian orbital frequency around the star of a mass M_*, and $\delta v_\phi = v_\phi - r\Omega$ the deviation of the rotation velocity to the Keplerian velocity. Following the paradigmatic definition of Shakura-Sunyaev of the radial stress tensor and expanding it to the vertical stress tensor, we define dimensionless parameters that quantify the magnitude of the stress tensors as

$$\begin{aligned} \alpha_{\rm SS} &\equiv \frac{2}{3}\frac{\int T_{r\phi}dz}{\Sigma c_s^2} = \frac{2}{3\sqrt{2\pi}}\frac{\int T_{r\phi}dz}{HP_0}, \\ \alpha_{\rm DW} &\equiv \frac{4}{3}\frac{r|T_{z\phi}|_{-H_W}^{+H_W}}{\Sigma c_s^2} = \frac{4}{3\sqrt{2\pi}}\frac{|T_{z\phi}|_{-H_W}^{+H_W}}{\epsilon P_0}. \end{aligned} \tag{2.2}$$

One can already notice that $\alpha_{\rm DW}$ is proportional to the disk magnetisation, i.e. the ratio between the mid-plane magnetic and thermal pressure. We further assume that the specific angular momentum in the MHD wind is $j_W = \lambda j_K$, where j_K is the Keplerian angular momentum at the footpoint of the wind. λ is called the magnetic lever arm parameter and has the major advantage of being observationally constrained by the measurement of wind rotations. Injecting this definition and Eq (2.2) into Eq. (2.1), we finally get the master equation describing how the disk surface density evolves

$$\frac{\partial \Sigma}{\partial t} = \frac{3}{r}\frac{\partial}{\partial r}\left\{\frac{1}{r\Omega}\frac{\partial}{\partial r}\left(r^2\alpha_{\rm SS}\Sigma c_s^2\right)\right\} + \frac{3}{r}\frac{\partial}{\partial r}\left\{\frac{\alpha_{\rm DW}\Sigma c_s^2}{\Omega}\right\} - \frac{3\alpha_{\rm DW}\Sigma c_s^2}{(\lambda-1)r^2\Omega}. \tag{2.3}$$

This equation is a generalization of the standard disk equation.

2.2 Analytical solutions

At this stage, one can prescribe any magnitude and functional form for $\alpha_{\rm DW}$, $\alpha_{\rm SS}$, and λ, and solve Eq. (2.3) numerically (see e.g., Zagaria et al. 2022). However, in our work, we were able to find analytical solutions assuming simple but physically motivated prescriptions on $\alpha_{\rm DW}$, $\alpha_{\rm SS}$, and λ. This allows us to highlight the essential features of MHD wind-driven accretion. By analogy with the solutions of Lynden-Bell & Pringle (1974), the surface density follows a self-similar form with

$$\Sigma(r,t) = \Sigma_c(t)\left(\frac{r}{r_{\rm c}(t)}\right)^{-1+\xi} e^{-r/r_{\rm c}(t)}, \tag{2.4}$$

where ξ is the mass ejection index, $r_{\rm c}(t)$ is the characteristic disk radius, and $\Sigma_{\rm c}(t)$ is the characteristic surface density. In the absence of radial transport of angular momentum ($\alpha_{\rm SS} = 0$), $\xi = 1/[2(\lambda-1)]$ (see Lynden-Bell & Pringle 1974, for the general expression).

We further assume that $\alpha_{\rm SS}$ and λ are constant in time and across the disk*. $\alpha_{\rm DW}$ is assumed to be constant across the disk and, in Tabone et al. (2022a), we explore in two classes of solutions:

1. Hybrid case with constant $\alpha_{\rm DW}$ and $\alpha_{\rm SS}$ parameters. This class of solutions highlights the role of radial transport compared with vertical transport.

2. Pure wind solutions with $\alpha_{\rm DW}(t) \propto \Sigma_{\rm c}(t)^{-\omega}$, where $\omega > 0$ is a free parameter. $\alpha_{\rm DW}$ being proportional to the local disk magnetization, this class of solutions highlights the major impact of the secular evolution of the magnetic field, a process that remains poorly constraints by numerical simulations (Lesur+2022).

*Analytical solutions with a radial power-law dependence of $\alpha_{\rm DW}$ and $\alpha_{\rm SS}$ are presented in Tabone et al. (2022a)

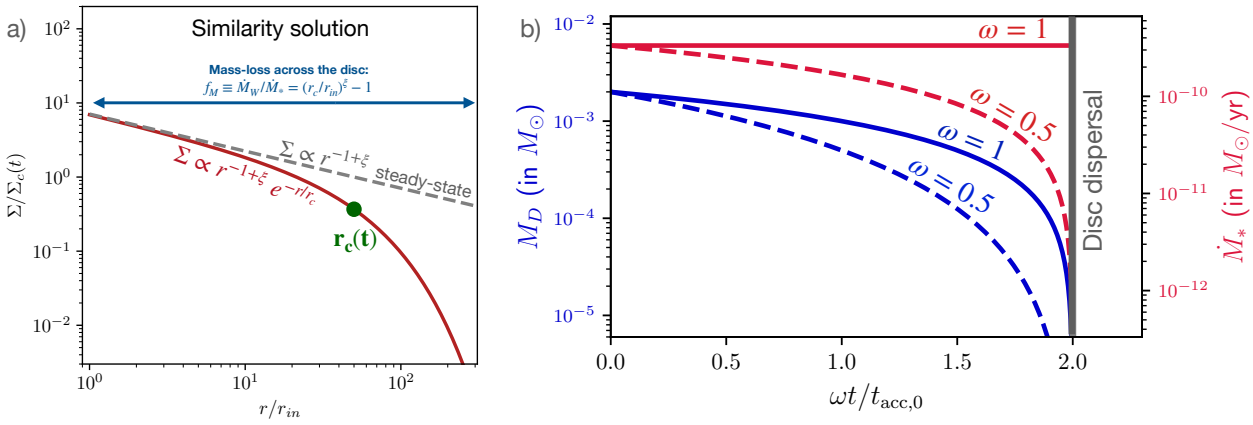

Fig. 1. Analytical solutions for the secular evolution of an MHD wind-driven disk. a) Surface density profile of the self-similar solution. The surface density profile keeps the same shape as the disk evolves: it is a power-law tapered by an exponential at large distance. b) Evolution of the disk mass for the Σ_c-dependent $\alpha_{\rm DW}$ case for two values of ω. A full dispersal of the disk is seen at $t_{disp} = 2t_{\rm acc,0}/\omega$. Adapted from Tabone et al. (2022a,b).

In this contribution, we focus only on the latter class of solutions because it is only those which predict the full dispersal of the disk after a finite time. The evolution of the disk mass and accretion rate for the pure wind solutions can be obtained by injecting the ansatz Eg (2.4) into Eq. (2.3). After some algebra, one can show that the disk mass and accretion rate is

$$\begin{aligned} M_D(t) &= M_0 \left(1 - \frac{\omega}{2t_{\rm acc,0}} t\right)^{1/\omega}, \\ \dot{M}_*(t) &= \frac{M_0}{2t_{\rm acc,0}(1+f_M)} \left(1 - \frac{\omega}{2t_{\rm acc,0}} t\right)^{-1+1/\omega}, \end{aligned} \tag{2.5}$$

where $f_M \equiv \dot{M}_W/\dot{M}_* = (r_c/r_{in})^\xi - 1$ is the mass ejection-to-accretion ratio, $t_{\rm acc,0} \equiv \frac{r_c}{3\epsilon_c c_{s,c}\alpha_{DW}(0)}$ is the initial accretion timescale (a generalisation of the viscous timescale), and ϵ_c and $c_{s,c}$ are the disk aspect ratio and the sound speed at $r = r_c$. Therefore, $M_D(t)$ and $\dot{M}_*(t)$ are controlled by four independent parameters: M_0, f_M, $t_{\rm acc,0}$, and ω.

Figure 1-b and Eq. (2.5) show that the disk mass drops to zero after a finite time called the disk dispersal time. This remarkable behaviour, in stark contrast with purely viscous disks for which the mass and accretion rate decrease smoothly without being fully dispersed. A more detailed analysis of the solutions show that this behaviour is due to the fact that (1) for pure wind-driven accretion, the disk size is constant, allowing for the full draining of the disk, and (2) for the Σ_c-dependent wind torque solutions, $\alpha_{\rm DW}$ increases with time, driving disk accretion with an increased efficiently. The latter feature mimics the increase in disk magnetization as the gas density declines faster than the strength of the magnetic field.

Therefore, our Σ_c-dependent wind torque solutions describe two different features of the disk evolution: disk dispersal, and disk accretion. Both processes that have been interpreted in the past as two distinct processes (turbulent accretion and photoevaporation) are link here by the same process: the wind-driven accretion. Interestingly, both processes are controlled by a single timescale: the accretion timescale $t_{\rm acc,0}$, with $t_{disp} = t_{\rm acc,0}/2\omega$, and the ratio between disk mass and accretion rate (often called "disk lifetime") proportional to $t_{\rm acc,0}$. In turn, it means that there are little freedom in the models when comparing to the observations.

3 Synthetic disk populations and comparison with disk surveys

In the observations, we never follow the secular evolution of a single disk on a Myr timescale but rather the statistical properties of disk populations of different ages. This means that in order to confront the predictions of a model to the observations, a population synthesis approach has to be adopted, namely a model that follows a population of disks that are born with different initial conditions. This approach is relatively new in the disk community (Lodato et al. 2017) but somewhat similar to the well developed stellar or planet population synthesis models (Mordasini 2018). Within the framework of our model, the evolution of the mass and accretion rate of an individual disk is dictated by 4 free parameters: M_0, $t_{\rm acc,0}$, ω, and f_M. We assume that ω and f_M are the same within a disk population. Our disk population model is then

defined by an initial distribution of M_0 and an initial distribution of $t_{\rm acc,0}$. In Tabone et al. (2022b), we constrain these distributions following a two step approach: first fitting the distribution of $t_{\rm acc,0}$ from the observed disk fractions, and secondly, comparing the predicted accretion properties to those observed.

Disk dispersal Extensive surveys show that the fraction of young stars with infrared excess or accretion signatures drops with the cluster age over a typical time of about 2-3 Myr (see Fig. 2-a). Our disk evolution model predicts that a disk is fully dispersed after $t_{disp} = 2t_{\rm acc,0}/\omega$ (see Fig. 1-b). We can therefore reconsider the decline of disk fraction with cluster age as the result of a distribution in initial $t_{\rm acc,0}$. For example, the fact that 30% of young star host a disk after 6 Myr points toward a population that had initially 30% of disks born with $t_{disp} = 2t_{\rm acc,0}/\omega > 3$ Myr. Following this approach, we determine the distribution of $t_{\rm acc,0}$ that fits the disk dispersal time (see Fig. 2-a-b). At this stage, this is not a comparison to the data but a fit to the data. However, as soon as we prescribe a distribution in $t_{\rm acc,0}$, the accretion properties of the population are somewhat constrained since $M_D/\dot{M}_* \propto t_{\rm acc,0}$.

Correlation between disk masses and accretion rates One of the most striking observational results of the past decade has been the discovery of a correlation between accretion rates and disks masses estimated from the mm continuum fluxes (Manara et al. 2016). The accretion rates are found to be on average nearly proportional to the estimated disk mass, with a large scatter around the main trend (see Fig. 2-c). In order to confront our prediction to these observations, we use the unique dataset compiled by Manara et al. (2019) on the 2 Myr old Lupus star-forming region. Since the distribution of $t_{\rm acc,0}$ is already set by the requirement to fit disk dispersal, we only have to further assume a distribution of initial disk mass, and a value for f_M, the ejection-to-accretion mass ratio. Figure 2-c shows the predicted distribution of the synthetic disk population in the $M_D - \dot{M}_*$ plane using the distribution of Class I disk mass derived from ALMA and VLA surveys (Tychoniec et al. 2020). Our model reproduces remarkably well the data. The $M_D - \dot{M}_*$ correlation is recovered. The scatter of the data around the mean trend is also reproduce, a feature that is difficult to reconcile will viscous disk models (Lodato et al. 2017; Sellek et al. 2020). Finally, the median value of the $M_D/\dot{M}_*$ ratio is well reproduce. In fact, this value depends on the f_M parameter that controls the mass lost in the wind and therefore the value of the accretion rate. A value of $f_M = 0.6$ is needed to reproduce the data.

Rapidity of disk dispersal Disk dispersal is also known to be a fast process: after a few Myr, the disk is quickly dispersed within $\lesssim$0.5 Myr. In this work, we have also checked that our synthetic population reproduces the rapidity of disk dispersal. Without any further adjustment, we naturally reproduce the distribution of disk mass around stars more massive than $0.6 M_\odot$, and in particular the scaricity of low mass disks. This is indeed a stringent test because if the disk were to disperse slowly they would have been distributed all the way down to the detection threshold, which is not what is observed (see Fig. 4 in Tabone et al. 2022b).

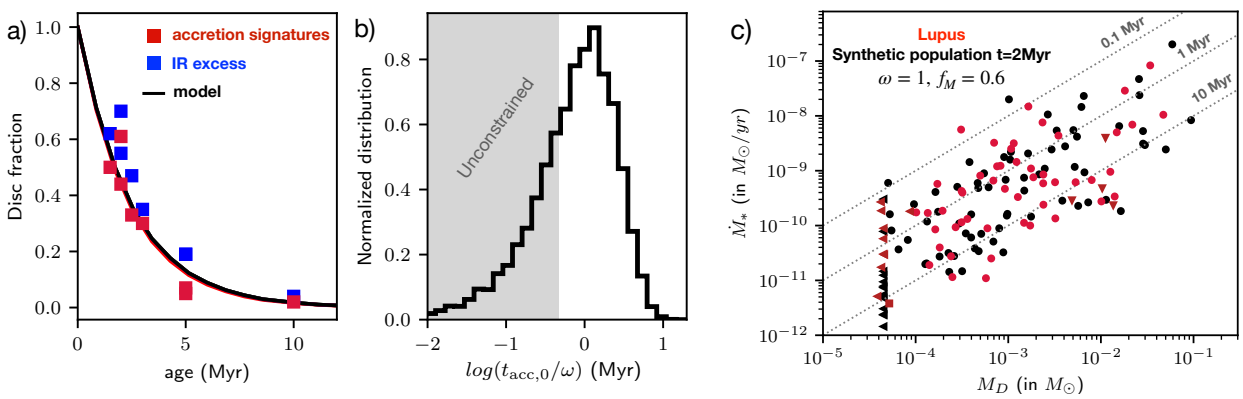

Fig. 2. Comparison between our synthetic disk population and the observational data. a) Decline of disk fraction with cluster age (from Fedele et al. 2010), with the fit adopted in our model. By construction, our synthetic population always fits the disk fraction. b) Inferred distribution of $t_{\rm acc,0}$ required to fit the disk fraction. c) Correlation between disk mass and accretion rate as measured in Lupus (red, data collected by Manara et al. 2019) and as predicted by the model (black). Figures from Tabone et al. (2022b).

4 Concluding remarks

In this contribution, we re-analyze the observational results on disk demographics from the new vantage point of wind-driven accretion. The paradigmatic viscous model of Shakura-Sunyaev is extended to include MHD disk-winds and construct analytical solutions. A synthetic disk population approach is then developed to compare our model with the recent surveys of star forming regions. We show for the first time that wind-driven accretion can naturally explain both disk dispersal and the observed correlation between accretion rates and disk masses (Tabone+2022b) without the need for photoevaporation to disperse the disk. The model also accounts for the rapidity of the disk dispersal. This paves the way for planet formation models in the paradigm of wind-driven accretion.

We however insist on the fact that our work does not exclude the alternative scenario, namely the viscous scenario with internal photoevaportation (or any hybrid scenarios). We only show that MHD disk winds is a compelling mechanism able to reproduce the main features of disk demographics with very little adjustments. The next challenges will be to discriminate viscous evolution from MHD wind-driven evolution. Whereas both wind-driven and viscous models can reproduce the disk fractions and the accretion properties, we predict that in the absence of radial transport of angular momentum, the disk sizes remain constant. This discriminant diagnostics will be soon available thanks to the AGE-PRO ALMA large programme (PI: K. Zhang), that will systematically measure the disk gas size in a sample of 30 disks in 3 regions of different ages.

References

Béthune, W., Lesur, G., & Ferreira, J. 2017, A&A, 600, A75

Fedele, D., van den Ancker, M. E., Henning, T., Jayawardhana, R., & Oliveira, J. M. 2010, A&A, 510, A72

Lesur, G., Ercolano, B., Flock, M., et al. 2022, arXiv e-prints, arXiv:2203.09821

Lodato, G., Scardoni, C. E., Manara, C. F., & Testi, L. 2017, MNRAS, 472, 4700

Lynden-Bell, D. & Pringle, J. E. 1974, MNRAS, 168, 603

Manara, C. F., Ansdell, M., Rosotti, G. P., et al. 2022, arXiv e-prints, arXiv:2203.09930

Manara, C. F., Mordasini, C., Testi, L., et al. 2019, A&A, 631, L2

Manara, C. F., Rosotti, G., Testi, L., et al. 2016, A&A, 591, L3

Morbidelli, A. & Raymond, S. N. 2016, Journal of Geophysical Research (Planets), 121, 1962

Mordasini, C. 2018, in Handbook of Exoplanets, ed. H. J. Deeg & J. A. Belmonte, 143

Sellek, A. D., Booth, R. A., & Clarke, C. J. 2020, MNRAS, 498, 2845

Shakura, N. I. & Sunyaev, R. A. 1973, A&A, 500, 33

Tabone, B., Rosotti, G. P., Cridland, A. J., Armitage, P. J., & Lodato, G. 2022a, MNRAS, 512, 2290

Tabone, B., Rosotti, G. P., Lodato, G., et al. 2022b, MNRAS, 512, L74

Tychoniec, Ł., Manara, C. F., Rosotti, G. P., et al. 2020, A&A, 640, A19

Zagaria, F., Rosotti, G. P., Clarke, C. J., & Tabone, B. 2022, MNRAS, 514, 1088